Correlation of microseismic and chemical properties of brittle deformation in Locharbriggs sandstone

Ira O. Ojala, Bryne T. Ngwenya, Ian G. Main, and Stephen C. Elphick

School of GeoSciences, University of Edinburgh, Edinburgh, UK

[1] The time-dependent properties of ceramic materials such as rocks depend both on preexisting cracks and chemical properties acting at their tips. We have examined the direct effect of chemical processes on the growth of a crack population by carrying out triaxial flow-through compression tests on Locharbriggs sandstone. The tests were carried out at temperatures of $25-80°C$ and at strain rates ranging from 10^{-5} to 10^{-8} s^{-1} under constant stress rate loading. The exit pore fluid was analyzed after the tests for the concentration of dissolved ions and acoustic emission was monitored in real time throughout the tests. The exit pore fluid silica concentration and microcrack damage derived from the acoustic emission (AE) data both exhibited an exponential increase during the strain hardening phase of deformation. Damage parameters inferred from the AE data predict the stress-strain curves adequately, or at least up to the point of strong microcrack coalescence. The damage parameters and silica signal were strongly correlated by a power law relationship. The observed environment and strain rate dependence of mechanical properties can hence be attributed uniquely to time-dependent crack growth by the stress corrosion mechanism. *INDEX TERMS:* 1045 Geochemistry: Low-temperature geochemistry; 5102 Physical Properties of Rocks: Acoustic properties; 5104 Physical Properties of Rocks: Fracture and flow; *KEYWORDS:* stress corrosion, acoustic emission, silica dissolution, subcritical crack growth, deformation rate, brittle fracture

1. Introduction

[2] Water is ubiquitous in the Earth's crust. It plays an active role in the mechanical, thermal and chemical processes operating in the crust. In the temperature and pressure conditions of the upper crust, rocks deform in a brittle fashion. The presence of water influences the brittle deformation properties of rocks in two ways. The poroelastic effect results from changes in pore pressure that affect the local effective pressure. Second, chemical weakening of the strained crack tip bonds may facilitate crack propagation. This mechanism is known as stress corrosion [*Anderson and Grew*, 1977; *Atkinson*, 1982, 1984]. It causes brittle fracturing process to be time-dependent as long as a rock is subjected to a reactive environment.

[3] Because of the abundance of silica in the crustal setting it is the time-dependent behavior of the quartz-water system that is of particular importance. The long-term evolution of hydrocarbon reservoirs, hydrothermal deposits and waste repositories is likely to be influenced by the physico-chemical processes that govern the mechanical properties of quartz. In fact, subcritical crack growth by stress corrosion or dissolution is probably the dominant mechanism of fracture nucleation in the upper crust [*Ander-son and Grew*, 1977; *Barnett and Kerrich*, 1980; *Crampin et al.*, 1984; *Atkinson and Meredith*, 1987a; *Renshaw and Pollard*, 1994]. Therefore it is not surprising that both the time-dependent fracturing properties of quartz [*Scholz*, 1972; *Martin*, 1972; *Dunning et al.*, 1980, 1984; *Atkinson*, 1984; *Kirby*, 1984] and the associated silica dissolution [*Rimstidt and Barnes*, 1980; *Paterson*, 1986; *Brady and Walther*, 1990; *Dove and Crerar*, 1990; *Berger et al.*, 1994; *Dove*, 1994, 1995; *Dove and Rimstidt*, 1994; *Franklin et al.*, 1994] have received much attention in the literature. The general consensus is that the fracturing process in glassy and crystalline silicates proceeds via the rupture of Si-O bonds at crack tips and that these rupture rates are accelerated when the crack tip bonds are strained by external stresses. Although the close resemblance of chemical reaction to brittle fracture propagation has long been recognized [*Krausz and Eyring*, 1975; *Krausz*, 1978; *Darot and Gueguen*, 1986], it was not until recently that *Dove* [1995] pinpointed that both stress corrosion fracturing and silica dissolution are described by identical equations. In general, silica dissolves in water by the reaction

$$SiO_2(s) + 2H_2O(l) = H_4SiO_4(aq) \qquad (1)$$

where the particular form of (1) is governed by the type of water (molecular or ionized) involved [*Dove*, 1994, 1995]. By linking both physical and chemical controls on stress
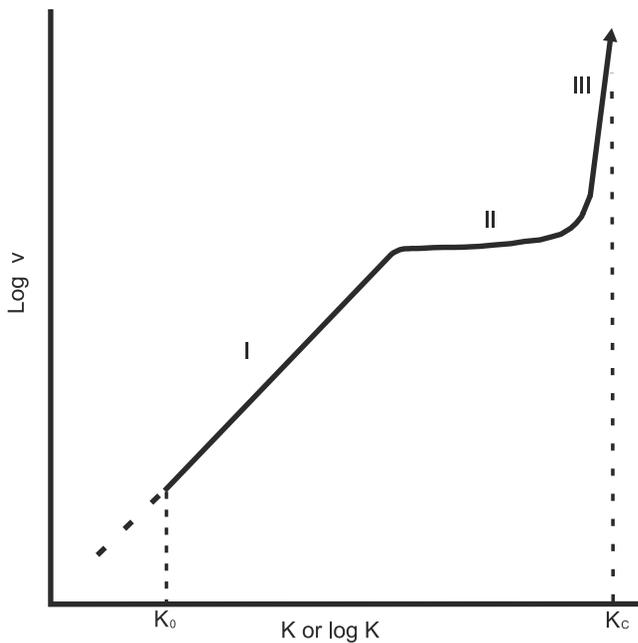
Figure 1. Schematic curve that relates stress intensity K to crack velocity v (redrawn from *Lockner* [1993b]).

corrosion crack growth in the quartz-water system, *Dove* [1995] developed a kinetic model that accounts for the observed variation in crack growth rates associated with humidity, pH and temperature. However, even in the absence of dissolution from crack tips, one might expect a geochemical signal associated with dissolution from the newly created fracture surface. The motivation for our study is to quantify the extent of microcracking and investigate whether such fracturing is associated with an elevated silica dissolution during time-dependent deformation in a quartz-rich sandstone in an aqueous environment.

[4] Time-dependent deformation by the stress corrosion mechanism is termed 'subcritical' since it refers to stable, quasi-static crack growth below a critical value K_c or G_c of the stress intensity factor K or the strain energy release rate G, respectively. While K is a local parameter describing the crack tip force field, G is a global parameter that is related to the crack growth energetics. Under plane stress conditions the stress intensity factor K_I(2) for mode I crack growth and the relationship between K_I and G_I are given by [*Lawn*, 1993]

$$K_I = Y\sigma c^{1/2} \qquad (2)$$

$$G_I = K_I^2/E \qquad (3)$$

where σ is the remotely applied stress, E is Young's modulus and Y is a dimensionless geometric constant. In laboratory environment such quasi-static crack growth for $K < K_c$ is conveniently measured by carrying out a double torsion or a double cantilever test [*Atkinson and Meredith*, 1987b]. Such loading configuration allows the direct measurement of crack velocity as a function of the applied stress intensity. The classic trimodal behavior observed for

stress corrosion in a monominerallic glass is illustrated in Figure 1. In region I the crack growth velocity v is controlled by the rate of chemical reactions at the crack tip. In region II, v is controlled by the transport of reactive species to the crack tip. In region III, v is relatively insensitive to the chemical environment. Usually, only region I type behavior is observed for rocks.

[5] Subcritical crack propagation is characteristically very sensitive to the applied load (Figure 1) and therefore many kinetic laws of crack growth describe the crack growth velocity v as a function of K or G [*Anderson and Grew*, 1977; *Atkinson*, 1982; *Atkinson and Meredith*, 1987a]. The most commonly used expressions for region I (Figure 1) subcritical crack growth velocities include the *Charles* [1958] power law and the *Wiederhorn and Boltz* [1970] and *Lawn* [1993] exponential laws. In terms of K and G, these can be written as

$$V = V_0(K/K_0)^n \qquad (4)$$

$$V = V_0 \exp(\alpha K) \qquad (5)$$

$$V = V_0 \exp(\beta G) \qquad (6)$$

respectively, where n is termed the subcritical crack growth index and α, β are constants. While the exponential form (5) is derived from reaction rate theory for the propagation of a single crack [*Charles and Hillig*, 1962; *Wiederhorn and Boltz*, 1970; *Lawn*, 1993], the power law (4) is consistent with the growth of multiple cracks in stochastic granular medium [*Main*, 1999]. Other workers have suggested an exponential dependence on G rather than K and based their argument on reaction rate theory [*Darot and Gueguen*, 1986], adsorption theory [*Dunning et al.*, 1984] and the quasi-static growth of Griffith cracks [*Rice*, 1978]. In previous studies, both power law [*Meredith and Atkinson*, 1983; *Atkinson*, 1984; *Swanson*, 1984] and exponential [*Scholz*, 1972; *Martin*, 1972] forms have been used to describe the crack growth data. However, for most polycrystalline rocks the value of the exponent n ranges from 30 to 60 [*Atkinson and Meredith*, 1987b]. Because of this very strong dependence of v on K it may not be possible to distinguish between equations (3), (4) and (5) when describing experimental data over a narrow range of K values. For crack growth by the stress corrosion mechanism in aqueous environments the exponential law has better theoretical basis for the growth of a single crack [*Atkinson*, 1982; *Freiman*, 1984; *Lockner*, 1993b; *Dove*, 1995], while the power law is easier to incorporate into time-dependent predictive failure models [*Das and Scholz*, 1981; *Lankford*, 1981; *Sano et al.*, 1981; *Meredith et al.*, 1990; *Schultz*, 2000] and for the growth of a crack population.

[6] Recording acoustic emissions (AE) generated by propagating microcracks provides an indirect way to monitor crack growth in a triaxially loaded rock sample, although only a fraction of cracks is likely to be accompanied with a detectable AE [*Lockner*, 1993a]. In a typical test the dilatant phase of microcracking is marked by a rapid increase in AE event rate [*Obert and Duvall*, 1942; *Mogi*, 1962; *Scholz*, 1968]. Microfracturing activity can be inves-

tigated in terms of instantaneous and cumulative properties derived from the AE data set. While the AE event rate is directly proportional to the crack growth velocity [*Meredith and Atkinson*, 1983], the cumulative AE count obeys a linear relationship with inelastic volumetric strain [*Scholz*, 1968; *Sano et al.*, 1981] and is hence an appropriate damage parameter.

[7] We have used the AE technique to study the time dependent deformation characteristics of Locharbriggs sandstone under triaxial compression. We chose this material since its behavior has been well characterized in our previous work [*Mair et al.*, 2000; *Ngwenya et al.*, 2000]. The sensitivity of the microfracturing process to external parameters was quantified by varying the test environment, temperature and loading rate. The experiments were carried out under constant flow-through conditions, which allowed subsequent chemical analysis of the exit pore fluid.

[8] Experimental studies on dissolution of silicates and other oxides have shown that dissolution rates depend on the available surface area in contact with the fluid [*Rimstidt and Barnes*, 1980; *Parks*, 1984; *Holdren and Speyer*, 1987]. Higher surface area exposes more reactive sites to the circulating fluid, hence increasing the dissolution rate. In most cases the measured dissolution rate is proportional to the surface area, although the measured surface area may be significantly different from the reactive surface area. During a triaxial compression test the growth of axial microcracks is expected to increase both fresh and total surface area. Dissolution, however, may occur preferentially at asperity contacts, such as crack tips, that have enhanced solubility due to higher contact pressures. In order to monitor the possible geochemical changes associated with the microfracturing process, the exit pore fluid was sampled and analyzed for the concentration of dissolved ions, including silica. It has been previously shown that, under static loading conditions, the formation of a fault in Locharbriggs sandstone is associated with an increased amount of silica in the exit pore fluid [*Ngwenya et al.*, 2000]. The results of our experiments demonstrate that the dilatant phase of microcrack growth is marked by and exponential increase in both silica concentration and AE event rate. The accumulated damage derived from the AE catalogue is strongly correlated with the measured geochemical signal by a power law relationship. These observations provide further evidence that deformation, fluid flow and chemical reactivity are strongly coupled processes in the brittle crust.

2. Methodology

[9] The sandstone used for this study was obtained from Locharbriggs quarry in Dumfries, southwest Scotland. Locharbriggs sandstone is a high porosity Permian aeolian sandstone with detrital mineralogy of quartz (88%) and K-feldspar (6%) [*Mair et al.*, 2000]. The diagenetic assemblage is characterized by hematite and illite coatings on the grain surfaces.

[10] Cylindrical samples measuring 80 mm in length and 38 mm in diameter were cut parallel and perpendicular to lamination from fresh, unweathered blocks of Locharbriggs sandstone. The ends were ground parallel and flat to produce precise right-angled cylinders. The total porosity of the sample was measured using the density method [*Gueguen and Palciauskas*, 1994]. The interconnected porosity was determined from the weight difference between a dry and saturated core. Typically, the total and interconnected porosities were 22% and 16%, respectively.

[11] The samples were deformed in a conventional triaxial ($\sigma_1 > \sigma_2 = \sigma_3$) testing apparatus under flow-through conditions at constant flow rate. The confining pressure was fixed within the brittle regime at 13.5 MPa and the ambient back pressure was 0.1 MPa. In order to investigate the time and temperature dependence of brittle deformation, dynamic tests were carried out at different loading rates and at temperatures of $25-80°C$. The four different loading rates used correspond to strain rates ranging from 10^{-5} to 10^{-8} s^{-1} during the linear elastic phase of deformation.

[12] To reduce frictional end effects, a thin sheet of melinex and a steel end piece was placed between the sample and the steel platen. The possible movement of larger particles that might have blocked the hydraulic system was prevented by inserting a nylon sheet between the specimen and the melinex sheet. The jacketed sample was heated to the appropriate temperature and initially loaded to hydrostatic conditions. Oil was used as the confining medium. In order to remove highly reactive fine particles the specimen was then flushed with distilled water for 24 hours at constant fluid flow rate Q = 0.2 mL min^{-1}. This is also the flow rate of water for the dynamic loading tests. The value of Q was dictated by the need to deliver an accurate and constant flow rate. Unfortunately, low Q value combined with short sample length resulted in linear flow velocities of 6.6 cm h^{-1} that were too high for the solution to reach equilibrium with the minerals in the rock specimen [*Ngwenya et al.*, 2000].

[13] The exit pore fluid was directed to an autosampler loaded with test tubes. The samples were acidified by using 1% HCl in order to prevent adsorption of dissolved species to container walls and to stop mineral precipitation. The pore fluid samples were analyzed after the tests for the concentration of Al, Ca, Fe, K, Mg, Na and Si by using atomic emission spectroscopy (ICP-AES). In order to obtain an adequate sample volume (5 mL) for analysis of dissolved species, sampling rates of once every 30 min and 1 hour were used. Consequently, a clear geochemical signal could only be recorded for the slower strain rate tests at 10^{-7} and 10^{-8} s^{-1}. To eliminate artifacts that might be produced by reactions in the experimental apparatus, a control test was carried out at hydrostatic conditions with distilled water directed through a nonreactive plastic specimen. Test results indicated that there was negligible dissolution of silica and iron from the stainless steel test apparatus. Hence all our results can be attributed to chemical dissolution within the rock core.

[14] The sampling times for the exit pore fluid were corrected for the residence time inside the rock specimen. Residence time τ describes the average time a fluid element resides inside the rock sample. Assuming constant porosity ϕ and constant fluid flow rate Q the residence time is given by

$$\tau = V_\phi/Q \qquad (7)$$

Table 1. Mechanical Data for Triaxial Flow-Through Compression Tests on Locharbriggs Sandstone[a]

Strain Rate $\dot{\varepsilon}$, s^{-1}	T, °C	Type	Failure Time t_f s	AE Events	Elastic Modulus, MPa	Peak Stress, MPa	Final Strain, %
3.0×10^{-5}	80	wet	596	3257	6219	81.2	1.96
3.1×10^{-6}	80	dry	5806	7812	6193	90.3	1.95
3.2×10^{-6}	80	wet	5519	948	6155	80.8	1.95
3.3×10^{-7}	25	wet	57495	4495	5252	81.3	2.08
2.8×10^{-7}	40	wet	64491	2788	5749	77.8	1.88
3.1×10^{-7}	60	wet	63980	1789	5401	81.4	2.12
3.4×10^{-7}	80	wet	70618	6541	5265	79.9	2.26
2.8×10^{-8}	80	wet	718414	922	5467	77.7	2.11
3.1×10^{-8b}	80	wet	655143	9818	5306	90.6	1.95

[a]Type indicates test environment.
[b]Denotes an experiment that was carried out on a specimen that was cut perpendicular to lamination. Therefore it is much stronger than the other specimens that were all cut parallel to lamination.

where V_ϕ is the pore volume. In analyzing the results, each chemical sample was plotted at a time when it resided halfway inside the rock sample. For a 8 cm long cylindrical sample with a 3.8 cm diameter and 16% interconnected porosity, the calculated pore volume is equaled 14.5 cm^3. Since a constant flow rate of 0.2 mL min^{-1} was used for all the tests, the average residence time given by equation (6) was 73 min.

[15] The acoustic emission (AE) activity was measured by a Panametrics 1 MHz piezoelectric transducer that was clamped at the bottom platen. In order to ensure a good contact with the transducer and the platen, honey was used as a couplant. The AE signals were amplified by 40 dB using a Panametrics preamplifier and recorded using MISTRAS acoustic emission system. To eliminate background noise the amplitude threshold for the AE signals was set at 50 dB. This is 10 dB higher than the amplitude threshold used in previous tests. Such higher than amplitude threshold was chosen in order to ensure adequate disk space for data storage, especially for the longer tests that lasted for several days. Because of the 50 dB amplitude threshold used, we expect the total number of AE events to be less than that of the previous studies.

3. Results

[16] Experiments were carried out in order to investigate the environment, strain rate and temperature dependence of brittle fracturing in sandstone. The mechanical data for nine Locharbriggs sandstone cores are summarized in Table 1. The effect of the test environment was first quantified by loading a water-saturated and an air-dry specimen under otherwise identical conditions. In the presence of water rock strength was reduced by 12%, as shown in Figure 2. In addition, the nonlinear part of the stress-strain curve, indicating yielding under strain hardening conditions began earlier and it was more pronounced for the wet specimen, indicating significant weakening of the rock imposed by the wet test environment. However, the total number of recorded AE events was greater for the dry sample. The greater number of AE events cannot be explained by the higher stresses sustained by the dry specimen since there is no correlation between the total number of AE events and specimen strength, as illustrated in Figure 3.
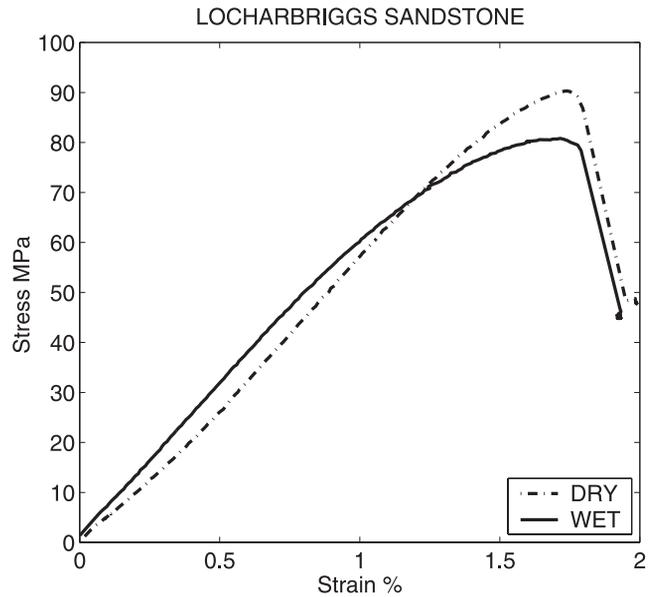

Figure 2. Stress-strain curves for a dry and a water-saturated sample that were loaded under otherwise identical conditions. The wet sample is considerably weaker than the dry one.

[17] The time dependence of rock strength was investigated by carrying out wet, flow-through tests at different loading rates. The corresponding strain rates range from the order of 10^{-5} to 10^{-8} s^{-1}, as shown in Table 1. With decreasing strain rate the rock strength (Figure 4) and elastic modulus were reduced (Table 1). Assuming that cracks grow by stress corrosion mechanism, equation (3) predicts a power law dependence of strength on deformation rate [*Lankford*, 1981; *Sano et al.*, 1981], while exponential [*Lockner*, 1998] and logarithmic formulae [*Segall*, 1984; *Reuschle et al.*, 1989] have also been suggested. However,
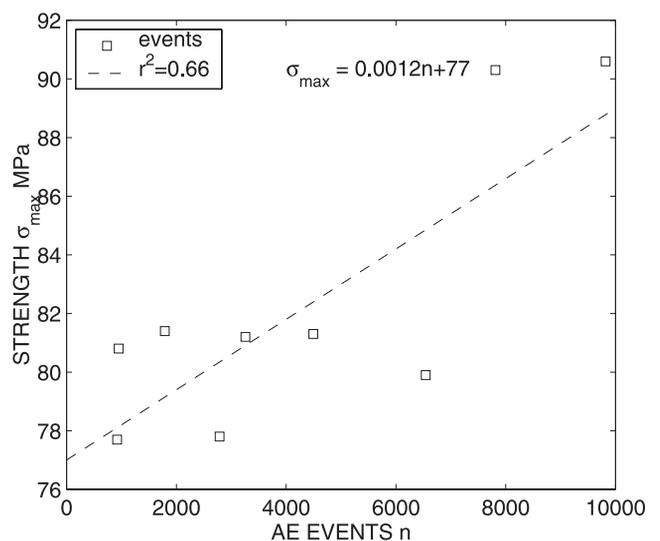

Figure 3. Peak stress sustained by a rock specimen as a function of total number of recorded AE events prior catastrophic failure. There is no correlation between specimen strength and the number of recorded AE events.
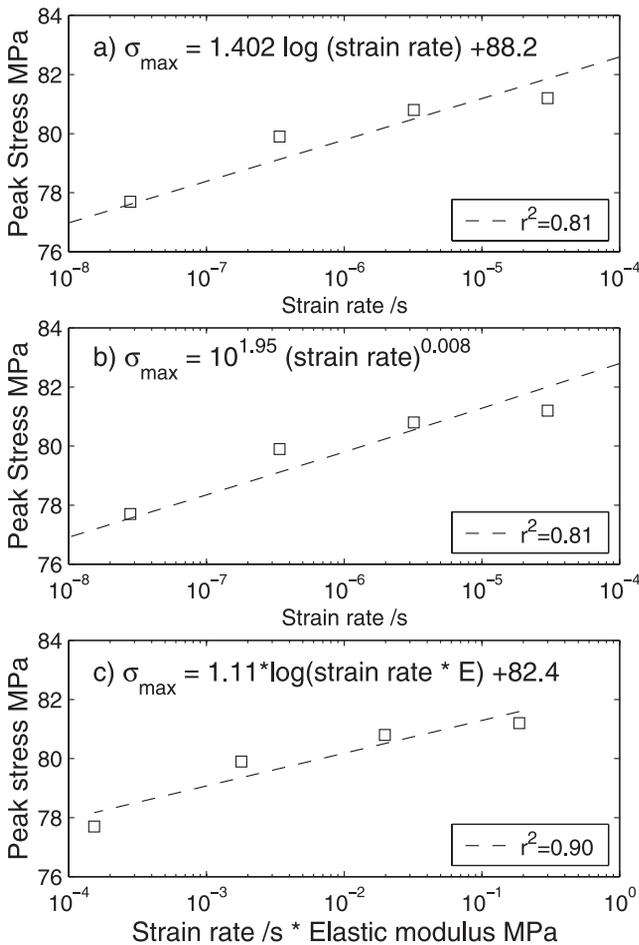
Figure 4. Strength of Locharbriggs sandstone as a function of strain rate. Both (a) exponential and (b) power law describe the data equally well. (c) However, rock strength is best predicted by assuming a logarithmic dependence on the product of strain rate and elastic modulus.

both power and logarithmic formulae described the data equally well, with an r-squared value of 0.81. We believe that the use of a power law is not justified here as the total variation in rock strength was less than one order of magnitude. In fact, specimen strength was best predicted by assuming a logarithmic dependence on both strain rate $\dot{\varepsilon}$ and elastic modulus E. Rock strength was proportional to the logarithm of $\dot{\varepsilon} * E$ with an r-squared value of 0.90. At lower strain rates the pore water has more time to reach the crack tips and undergo chemical reactions, which is a plausible explanation for the observed logarithmic decrease in rock strength. The observed reduction in E with strain rate also suggests more pervasive fracturing at slower strain rate tests, since the presence of cracks lowers the elastic modulus.

[18] The use of low loading rates for the tests allowed chemical changes to be measured. Since Locharbriggs sandstone is mainly composed of quartz, a clear geochemical signal was recorded for the variation of silica in the exit pore fluid. Figure 5 shows changes in axial stress, axial strain, acoustic emission (AE) activity and the concentration of silica for a flow through test at 80°C that was carried out

at a constant strain rate of 2.8×10^{-8} s^{-1}. The shape of the stress-strain curve (Figure 5) is characteristic of a rock sample subjected to a moderate confining pressure. Such stress-strain dependence is typically interpreted in terms of three microfracturing domains. Phase I depicts inferred compaction of favorably oriented microcracks and resulting increase in specimen stiffness. The linear elastic phase II is marked by a constant slope of stress versus strain. Phase II may not be truly linear elastic since AE events, indicating microfracturing inside the rock specimen, are frequently recorded during this stage [*Scholz*, 1968]. However, significant AE activity doesn't begin until at the yield point Y, that marks the onset of nonlinearity in the stress-strain relation. During phase III the rock becomes less stiff due to microcrack growth in the direction of maximum compressive stress [*Gueguen and Palciauskas*, 1994].

[19] During the early stages of loading (Figure 5) compaction of favorably oriented cracks lead to an exponential decrease in Si concentration in the exit pore fluid. Apparently, this reduction in surface area is dominant over pressure solution, which might be expected during compactive deformation at this temperature. There was no recorded acoustic emission activity during this stage. The linear
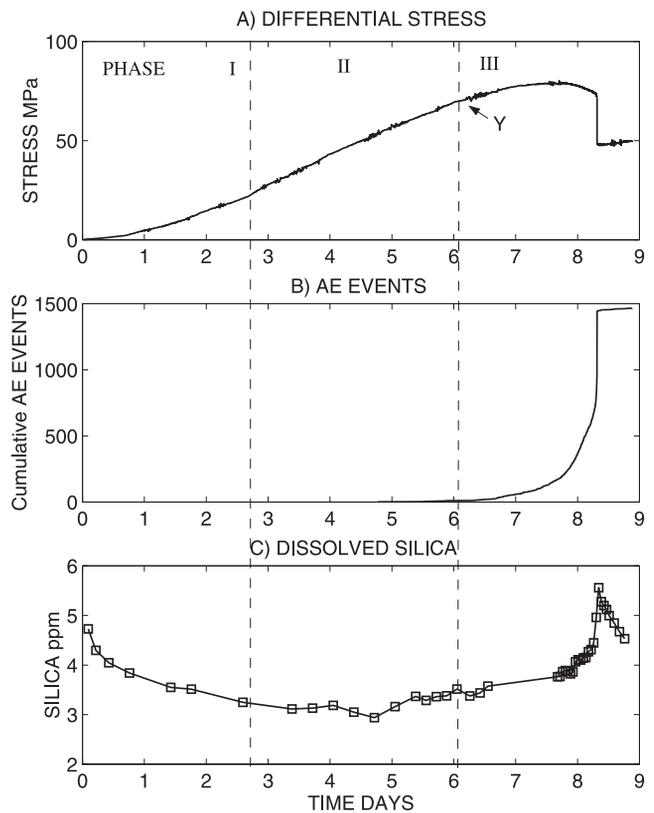

Figure 5. The measured (a) stress, (b) AE event rate and (c) exit pore fluid silica concentration as a function of time during slow loading of Locharbriggs sandstone. The strain rate used was 2.8×10^{-8} s^{-1}. The amount of dissolved silica in the exit pore water correlates with the three phases of microfracturing. These are inferred compaction (I), linear elastic phase (II) and strain hardening phase (III). Y indicates the yield point indicating the onset of nonlinearity in the stress-strain behavior.

elastic phase of deformation was marked by an approximately constant value of 3 ppm of dissolved silica and an intermittent, very low AE activity of 1 event per minute. Although both compactive and dilatant processes may be operating during this stage, the net increase in surface area can be considered to be zero. Consequently, it is not surprising that both Si concentration and AE activity assumed constant values during this stage. The constant value of dissolved Si can be considered to indicate a steady state in the dissolution reaction. The normalized reactive surface area s_n corresponding to the 3 ppm Si concentration was estimated from [*Kieffer et al.*, 1999]

$$s_n = \frac{\Delta C_{SiO_2} Q}{k_+ V_{rock}} \qquad (8)$$

where ΔC_{SiO_2} is the outlet silica concentration, Q is the mass fluid flow rate, k_+ is the normalized dissolution rate constant [*Rimstidt and Barnes*, 1980] and V_{rock} is the volume of the rock specimen. In comparison, a rough estimate of the specific surface area s_v of the rock specimen was obtained assuming regular packing of identical spheres given by

$$s_v = \frac{6(1 - \phi)}{D_p} \qquad (9)$$

where ϕ is the porosity and D_p is the pore diameter [*Dullien*, 1979]. For $\Delta C_{SiO_2} = 3$ ppm, $Q = 0.2$ mL min^{-1}, $k_+ = 4.79 \times 10^{-12}$ mol cm^{-2} s^{-1}, $V_{rock} = 90.7$ cm^3, $\phi = 16\%$ and $D_p = 200$ μm the calculated values were 0.38 and 252 cm^{-1} for s_n and s_v, respectively. Hence only a fraction of the total surface area was likely to be contributing to the measured silica signal at this deformation stage. This rules out the hypothesis that silica is dissolving passively from crack walls. However, the small reactive surface area is consistent with the stress corrosion mechanism.

[20] The following strain hardening phase of deformation was marked by rapid increase in both AE activity and silica concentrations. The increased amount of silica in the pore water can be attributed to dissolution from the crack tips or from the newly created fracture surfaces. The peak stress was followed by a pronounced period of strain softening indicating quasi-static crack linkage that eventually led to macroscopic failure and associated stress drop. Because of the modest confining pressure used the failure mode is a shear fault oriented at 40 ± 1 degrees to the cylinder axis, implying an internal friction coefficient of 0.8. The specimen failure was accompanied by a maximum in Si concentration due to dissolution from the newly created fault surface and gouge fill, as previously documented by *Ngwenya et al.* [2000]. Frictional sliding on a fault followed the macroscopic failure. During this stage the AE activity decreased to approximately constant level of 1 event per minute. Similarly, the concentration of Si in the exit pore fluid decreased during continued sliding on the newly created fault.

[21] Because of the requirement of 5 mL of sample for the ICP analysis, chemical changes could only be monitored for the slow strain rate tests at 10^{-7} to 10^{-8} s^{-1}. For all slow loading tests the variation in Si concentration corresponded to the three main stages of loading. An initial decrease

Table 2. Chemical and AE Data for the Triaxial Tests[a]

$\dot{\epsilon}$, s^{-1}	T, °C	Value	Fe, ppm	K, ppm	Na, ppm	Si, ppm	% AE Events After σ_{max}
3.3×10^{-7}	25	SS	0.1	-	0.8	0.3	74
		Max	1.2	0.8	1.9	0.8	
2.8×10^{-7}	40	SS	0.1	-	0.4	0.8	80
		Max	0.4	1.0	1.7	1.4	
3.1×10^{-7}	60	SS	1.0	0.5	0.8	1.7	60
		Max	2.1	2.2	2.6	2.7	
3.4×10^{-7}	80	SS	0.3	0.4	0.3	5.0	81
		Max	1.1	2.0	1.0	9.5	
2.8×10^{-8}	80	SS	0.1	0.6	0.5	3.0	91
		Max	0.3	1.3	0.7	5.5	
3.1×10^{-8}[b]	80	SS	0.1	0.2	0.2	3.4	61
		Max	0.1	1.7	1.0	6.7	

[a]The exit pore water contains dissolved silica, sodium, potassium and iron. During the linear elastic phase of deformation the concentration of dissolved ions is approximately constant, indicating a steady state. SS is the measured steady state value and dash indicates very low concentrations below 0.1 ppm. Majority of the AE events occur after the peak stress has been attained.
[b]This specimen was cut perpendicular, while the other specimen were cut parallel to lamination.

during inferred compaction was followed by steady state concentration and eventual increase in the amount of dissolved Si during the strain hardening phase of microcrack growth. Throughout the tests, minor amounts of Fe, K, Mg and Na were also present in the pore fluid, as illustrated in Table 2 and Figure 6. This observation can be attributed to dissolution from feldspar, dolomite and diagenetic hematite coatings on the quartz surfaces. This signal was stronger after the yield point, but the dissolution of Fe, K, Mg and Na was not directly correlated to the AE, possibly because of a much more complex chemical system, due to their higher surface to volume ratio or due to microfracturing events, that are not accompanied by a detectable AE. Consequently, for the remaining of the paper we will concentrate on the dissolution behavior of the dominant mineral (silica) and its correlation with the microseismic data. Since the Si concentration varied with temperature and strain rate (Table 2) a parameter ΔC_{Si} was defined as

$$\Delta C_{Si} = C_{out} - C^{ss} \qquad (10)$$

where C_{out} is the outlet silica concentration in ppm and C^{ss} is the steady state value for particular test as shown in Table 2. This allowed the comparison of data from different tests.

4. Data Analysis

4.1. Correlation of AE Damage With Stress and Chemical Reactivity

[22] The damage caused by microfracturing was quantified through various cumulative properties derived from the AE data set. We followed the methodology of *Cox and Meredith* [1993], who based their definition of a damage variable on the mean crack length derived from the AE catalogue. The damage parameter D, corresponding to the term χ' of *Cox and Meredith* [1993], is defined as

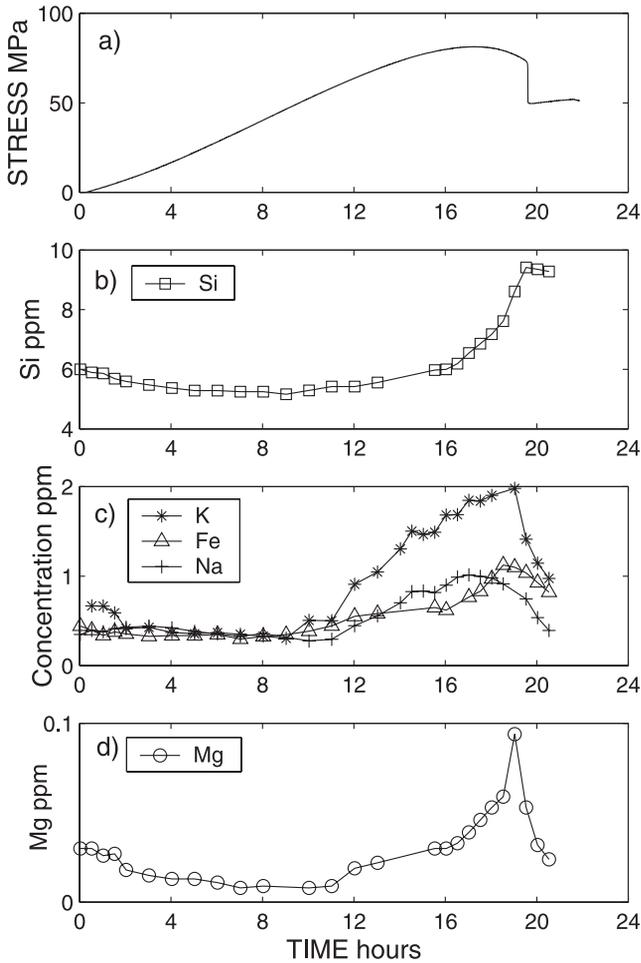$$D = \sum_{i=1}^{N} 10^{cm_i} \qquad (11)$$

Figure 6. The measured (a) differential stress and the exit pore fluid concentrations of dissolved (b) silica, (c) potassium, iron, sodium and (d) magnesium for a test conducted at 80°C with a strain rate of 3.4×10^{-7} s^{-1}. These data can be attributed to dissolution from feldspar, quartz, hematite and dolomite grains in the test specimen.

where c equals 1.5 for an AE sensor acting as a velocity transducer and m is the event amplitude in dB/20. While D can be considered to be proportional to the increase in fracture porosity (11), an additional fracture surface area parameter S was also derived. It was assumed that the S scales logarithmically with respect to event magnitude M_s, consistent with the dislocation theory for the seismic source [*Kanamori and Anderson*, 1975]. Hence the increase in fracture surface area S is given by

$$S = \sum_{i=1}^{N} (10^{cm_i})^{2/3} \qquad (12)$$

where c equals 1.5 (as above). It is assumed that S correlates with the increase in fracture surface area caused by microfracturing inside the rock sample. Furthermore, the cumulative event count N and the cumulative AE energy E were also derived from the AE data set. The parameter N scales linearly with the inelastic volumetric strain [*Scholz*, 1968; *Sano et al.*, 1981] and can thus be considered as a measure of the damage volume.

[23] To test the applicability of the newly defined indicators of damage, D, S, N and E were used to invert the measured stress-strain curves according to *Cox and Meredith* [1993]. In the inversion procedure they used the dilute crack model (13) of *Walsh* [1965] and the self-consistent *Bruner* [1976] model (14) in which the ratio of the modified stiffness E' to its initial value E is given by

$$\frac{E'}{E} = \frac{1}{1 + FD} \qquad (13)$$

$$\frac{E'}{E} = \exp(-HD) \qquad (14)$$

where F and H are scaling factors. Having obtained the value of E/E' the scaling factors F and H were determined from the linear portions of E/E' and $\ln E/E'$. versus D, respectively. Although the process of deriving the scaling factors was slightly circular, the derived values are unlikely to be wrong by more than a factor of two [*Cox and Meredith*, 1993]. Figure 7 shows typical inverted stress-strain curves. While *Cox and Meredith* [1993] used D to reconstruct the measured stress-strain curves, our result demonstrates that the cumulative energy E or the event count N can be used equally well in the inversion procedure. The main features of the stress-strain curves were reproduced using both Walsh and Bruner models and the damage parameters. However, during the later stage of loading both models consistently overestimated the peak stress, hence underestimating the amount of damage. This occurs as a result of high crack concentrations and crack linkage, that cannot be predicted using an isotropic damage
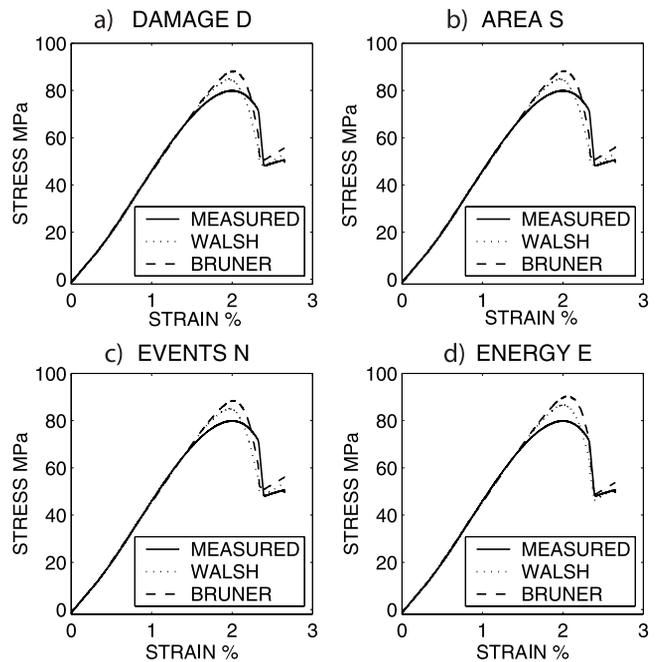

Figure 7. A plot of the inverted stress-strain curves using (a) D, (b) S, (c) N and (d) E as the working damage parameter in the models of *Bruner* [1976] and *Walsh* [1965]. All of the damage parameters derived from the AE data predict the measured stress-strain curves adequately.
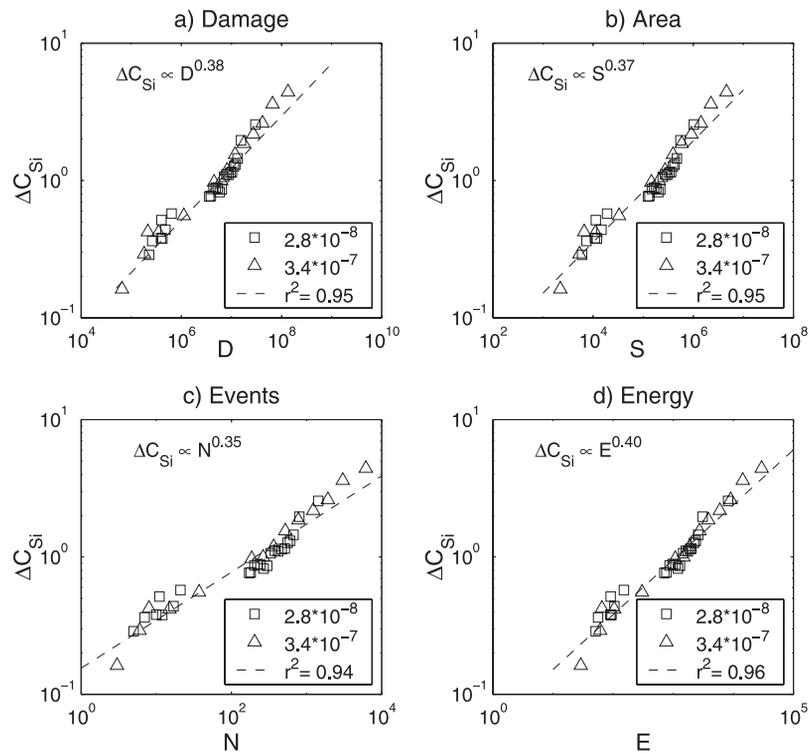
Figure 8. The measured amount of dissolved silica as a function of (a) damage D, (b) area S, (c) cumulative AE events N and (d) cumulative AE energy E. The damage parameters derived from the AE data and the amount of dissolved silica in the exit pore fluid are correlated by a power law relationship.

parameter suitable for dilute crack densities. Since the Bruner model does a better treatment of crack interactions the fit to the experimental data was better for this model. Damage is also likely to be underestimated due to the fact that AE is known to record only a fraction of cracks [*Lockner*, 1993a]. In deriving the models in Figure 7 we implicitly assumed that this fraction is a constant.

[24] The microfracturing damage D, S, N and E were found to be strongly correlated with the measured geochemical signal, as illustrated in Figure 8. Because of the temperature dependence of the dissolution process [*Dove and Rimstidt*, 1994], the best signal-to-noise ratio for the chemical data was obtained for the higher temperature tests. At 80°C the relationship between ΔC_{Si} and damage parameters D, S, E and N was best described by a power law of the form

$$\Delta C_{Si} \propto (D, S, N, E)^q \qquad (15)$$

where q is the power law exponent. In equation (10) the q value ranged from 0.35 to 0.40 with corresponding r-squared values of 0.94 to 0.96, respectively. The strong correlation between dissolved silica and microcrack damage is quantitatively consistent with the idea of progressive growth and linkage of microcracks by stress corrosion mechanism. The magnitude of the exponent q in the power law relation (15) indicates that only a proportion of the accumulated microcrack damage was chemically reactive at a given time. While S is a measure of the total increase in crack surface area, ΔC_{Si} is sensitive to the reactive surface area, which in turn, is a function of the connected

surface area accessible to the pore fluid. It is interesting to note that the cumulative energy E provided the best correlation with the measured Si signal. Similarly, for best fit to the measured data during stress history matching for the stress-strain behavior was obtained by parameter E. Although speculative, this may be an indication that the crack growth energetics are linked to the adsorption of environmental species onto the crack surface [*Dunning et al.*, 1984; *Parks*, 1984].

[25] The measured geochemical signal also displayed a distinct temperature dependence, as illustrated in Figure 9. Both steady state and maximum silica concentrations at specimen failure for the 25–80°C tests at 10^{-7} s^{-1} showed an Arrhenius type dependence on test temperature, indicating that reaction rates were also contributing to the measured Si signal. On the other hand, the steady state Si concentration C^{ss} at 80°C was not unique, as it was affected by the deformation rate (Table 2). For the 10^{-7} and 10^{-8} s^{-1} tests, the measured C^{ss} were 5.0 and 3.0 ppm, respectively. The lower steady state value at 10^{-8} s^{-1} could have been caused by greater initial compaction of the test specimen [*Sangha and Dhir*, 1972]. The Si concentrations are consistently below equilibrium concentrations due to the high linear flow velocity of the pore water [*Ngwenya et al.*, 2000].

4.2. Crack Growth Constitutive Equations

[26] The temporal evolution of the fracturing process was quantified through time to failure analysis of damage D, N and ΔC_{Si}. Assuming that cracks grow in a self-similar manner, the D and N can be considered as remote measures
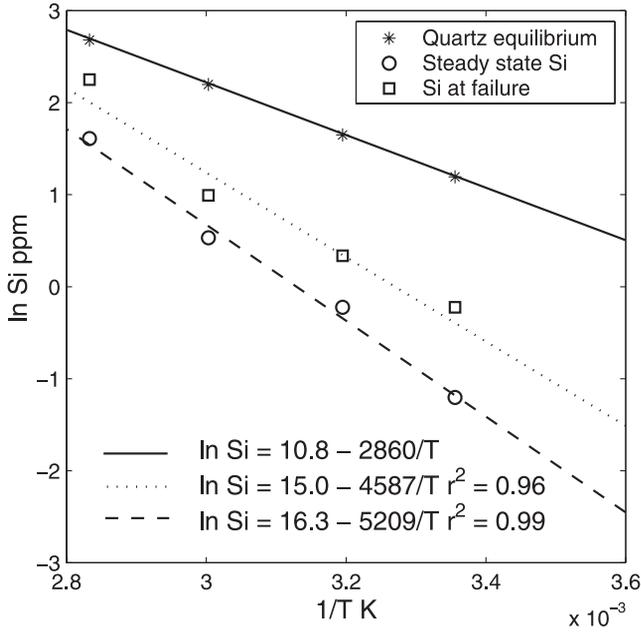
Figure 9. The steady state and peak silica concentrations for the slow strain rate as a function of inverse temperature for the slow strain rate tests at 10^{-7} s^{-1}. The concentrations display a clear temperature dependence. The equilibrium silica concentrations were calculated from *Rimstidt and Barnes* [1980].

of the mean crack length [*Main*, 1991; *Main and Meredith*, 1991] and the chemical reaction rate is also related to the macroscopic crack length [*Dove*, 1995]. For $n > 2$ the power law form (3) of the dependence of v versus $K(2)$ predicts the acceleration of crack length c at constant stress as follows:

$$c = c_0 \left(1 - t/t_f\right)^{2/(2-n)} \qquad (16)$$

where c_0 is the initial crack length at time t = 0 and t_f is the failure time [*Das and Scholz*, 1981; *Main*, 1999]. If the stress is increasing linearly, the resultant acceleration takes a similar form [*Main*, 2000] with a shorter acceleration for a given value of n. The exponential forms (4) and (5) predict a slightly different formula. Combining equations (2) and (5), we get

$$(dc/dt) = V_0 \exp(c/c*) \qquad (17)$$

where Y is a geometric factor, σ is stress and $c* = (Y^2\sigma^2\beta)^{-1}$. Integrating equation (17) and substituting $t_f = c*e^{c_0/c*}/V_0$ gives

$$c = c_0 - c * \ln\left(1 - t/t_f\right) \qquad (18)$$

[27]   Assuming that D and ΔC_{Si} are indicators of the mean crack length c, their evolution with time as predicted by equations (16) and (18) are investigated in Figure 10. While the chemical signal is well modelled by assuming exponential law (4), as indicated by the linear trend (Figure 10d), the accumulation of damage is not predicted best by either the exponential (16) or power law (18) formulation for subcrit-

ical crack growth. In fact, a good empirical fit to the measured damage can be provided by plotting log D versus (1-t/tf) as shown in Figure 10e. Such evolution of damage can be derived from the constitutive equations for subcritical crack growth by setting $n = 2$ in the power law formula (3) and thus

$$V = V_0(K/K_0)^2 \qquad (19)$$

which indicates that the crack growth rate is directly proportional to crack length c via

$$\frac{dc}{dt} = V_0(c/c_0) \qquad (20)$$

After integration the crack length is given by

$$c = c_0 \exp(V_0 t/c_0) \qquad (21)$$

Assuming that at $t = t_f$ the crack growth velocity v equals the Rayleigh wave velocity v_r the crack length c is given by

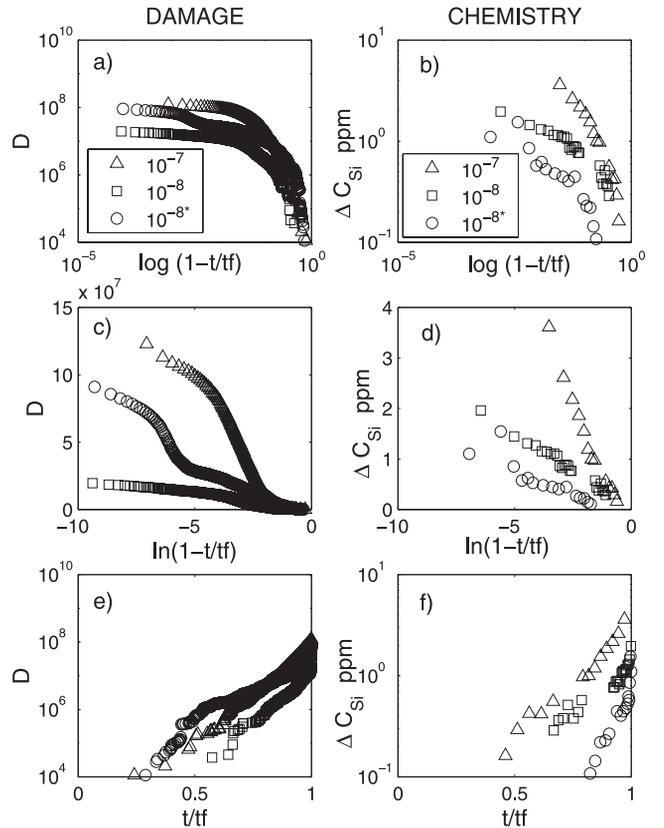$$c = c_0 \exp\left(p\frac{t}{t_f}\right) \qquad (22)$$

Figure 10. The temporal evolution of damage and silica content assuming (a, b) power law with $n > 2$, (c, d) exponential and (e, f) exceptional power law with $n = 2$ dependence of crack velocity v on stress intensity K. Both AE damage and chemical data are best described assuming v is proportional to K^2.

Table 3. Increase in Silica Concentration and Damage Which Obey an Exponential Law During the Strain Hardening Phase of Deformation[a]

$\dot{\varepsilon}$, s^{-1}	T, °C	$\Delta C_{Si}p$	r^2	Dp	r^2	Np	r^2
2.8×10^{-8}	80	4.26	0.904	14.4	0.982	16.3	0.989
3.1×10^{-8}[b]	80	11.4	0.874	8.13	0.958	8.34	0.969
3.4×10^{-7}	80	5.24	0.972	13.6	0.990	14.0	0.986
3.1×10^{-7}	60	8.25	0.786	3.51	0.811	3.29	0.810
2.8×10^{-7}	40	11.8	0.735	4.90	0.896	4.84	0.869
3.3×10^{-7}	25	22.0	0.950	6.01	0.938	6.38	0.942

[a]An exponential relationship is predicted assuming linear dependence of crack velocity v on stress intensity K. Here are the fitted values for the exponent p in equation (22) and the corresponding r-squared values for the different tests.

[b]This specimen was cut perpendicular to lamination. All the other samples used were cut parallel to lamination.

where p is a constant equal to ln (v_r/v_0). The specimen failure time t_f was marked by a maximum in AE event rate. Equation (22) provided the best fit to both crack damage and the measured Si signal, as indicated by the linear trend in Figures 10e and 10f. The temporal evolution D, E and ΔC_{Si} for temperatures of 25–80°C and $\dot{\varepsilon}$ of 10^{-7} to 10^{-8} s^{-1} could be expressed using (22) with high correlation coefficients (Table 3). The best fit was obtained for the 80°C tests, i.e., those which had the highest signal-to-noise ratio of the measured geochemical data. In fact, from Figure 10d it appears that Si dissolution could be equally well described using an exponential (13) formula. We believe that some of the apparent differences in the evolution of damage and ΔC_{Si} in Figures 10c and 10d can be attributed to the sampling frequency. While D was calculated from event rate per minute, the pore fluid was sampled every 30 min. Therefore the actual form of the constitutive time to failure equation is more difficult to resolve from the geochemical data.

5. Discussion

[28] The results of our experiments demonstrate that the strength of Locharbriggs sandstone is reduced in the presence of water and on the application of a lower loading rate. The observed environment and strain rate dependence of rock strength suggests subcritical crack growth by the stress corrosion mechanism, and it is accompanied by a close quantitative correlation between corrosion products, namely silica, and AE activity during the strain hardening phase of microcrack growth. This is perhaps not surprising because both the stress and resulting strain rates used for our experiments were chosen to lie in the region at which subcritical crack growth is considered to operate. The loading rates used for our experiments (1.2×10^{-4} to 1.5×10^{-1} MPa s^{-1}) are well below the suggested upper limit 10^5 MPa s^{-1} for stress corrosion crack growth [*John*, 1972; *Sano et al.*, 1981]. In fact, a reduction in rock strength by subcritical crack growth has been observed for strain rates as high as 10^{-3} to 100 s^{-1} [*Serdengecti and Boozer*, 1961]. For our experiments the strain rates range from the order of 10^{-5} to 10^{-8} s^{-1}. The results demonstrate that subcritical crack growth by stress corrosion mechanism is the cause of the observed environment and strain rate dependence of rock strength.

[29] The correlation between specimen strength σ_{max} and applied strain rate $\dot{\varepsilon}$ can be expressed in terms of a power or a logarithmic law with an identical r-squared value of 0.81. However, due to the small variation in rock strength amounting to less than an order of magnitude, the use of a power law is not appropriate. If the data is extrapolated to crustal strain rates of 10^{-16} s^{-1} an logarithmic law (Figure 4) predicts a 28% decrease in the strength of Locharbriggs sandstone at 80°C with 13.5 MPa confining pressure when compared to the ultimate dry σ_{max} at strain rate of 10^{-6} s^{-1}. Similar logarithmic reduction in rock strength has been predicted [*Mogi*, 1962; *Segall*, 1984; *Reuschle et al.*, 1989] and observed in granite and andesite specimen [*Mogi*, 1962; *Masuda*, 2001]. However, the best prediction of the rock strength is obtained by assuming a logarithmic dependence on a factor involving both strain rate and elastic modulus E (Figure 4c). As with the tests of *Sangha and Dhir*, [1972] on Laurencekirk sandstone, the elastic modulus of Locharbriggs sandstone also decreases with decreasing rate of deformation. The decrease in elastic modulus indicates a greater amount of damage in the slow strain rate tests that is likely to be caused by subcritical crack growth.

[30] Although there is little evidence for damage localization prior to dynamic stress drop [*Lei et al.*, 2000], it is generally agreed that propagation and coalescence of small fractures is the mechanism by which compressive deformation is accommodated in a rock specimen [*Gueguen and Palciauskas*, 1994]. The characteristic shape of the stress-strain curve may be interpreted in terms of changes in the spatial extent of such microfractures. Our results demonstrate that the measured geochemical signal also correlates with the three characteristic domains of a stress-strain curve. Compaction of pores and microcracks is associated with a decreasing concentration of Si while the following linear elastic phase is marked by an approximately constant concentration, indicating a steady state. The inferred dilatant phase of microfracturing associated with strain hardening by microcrack growth begins at the onset of significant AE activity and a concurrent increase in the amount of dissolved silica in the exit pore water is observed. The measured geochemical and microseismic signal are strongly correlated by a power law relationship (15). The strong correlation suggests that stress corrosion is the mechanism by which cracks are growing inside the rock specimen. However, it is important to recognize that while the AE event data is a measure of the total increase in crack porosity, the Si concentration relates to the amount of interconnected fracture surface area accessible to the pore fluid so that the exponent q between the Si signal and the inferred crack surface area need not to be unity. The existence of two distinct types of pore space was verified by initial porosity estimates, yielding 16% and 6% for the interconnected and unconnected porosity, respectively. Therefore some of the AE events may be attributed to the growth of microfractures from preexisting flaws outside the interconnected pore space. More importantly, the actual microcrack damage is likely to be underestimated by the AE catalogue [*Lockner*, 1993a] since all microfracturing events are not accompanied by a detectable AE and due to a higher amplitude threshold used for the tests. In addition, small otherwise unrelated events may overlap in time and hence be recorded as one long duration event. The stress

history matching exercise (Figure 7) demonstrates that damage is underestimated at a later loading stage. If a more realistic estimate of damage was available, one would expect a higher q values (Figure 8) linking damage to the chemical signal.

[31] In general, the dissolved Si concentration can be attributed to the reactive mineral surface area and dissolution/precipitation rates. Previous studies have suggested both linear [Kieffer et al., 1999] and exponential [Franklin et al., 1994; Ngwenya et al., 2000] dependence of the exit pore fluid silica concentration on the reaction rates (k_- or k_+) and the reactive surface area A_s. Although the surface area parameter S was estimated from the AE catalogue, the evolution of the interconnected surface area could not be measured independently during the triaxial tests. Therefore we cannot separate out the effects of surface area and reaction rates on the measured geochemical signal. The strong temperature dependence of the Si signal (Figure 9) as well as the low estimate of 0.38 cm^{-1} obtained for the reactive surface area suggest that reaction rates are dominating the measured silica concentrations. However, in the strain hardening and softening phases both Si concentrations and surface area parameter S evolve in a similar manner (Figure 8), suggesting surface area control. Hence we attribute the increase in dissolved Si during the dilatant microcracking phase to changes in both reaction rates and of the reactive surface area. It has been suggested that during stress corrosion, the propagation velocity of an individual crack can be equaled to the rate of chemical reaction at the crack tip [Wiederhorn and Boltz, 1970; Freiman, 1984], since dissolution is a likely result of the straining of the crack tip bonds. In such case both Si dissolution and fracture rates are governed the same rate constant k_+, the fraction of reactive sites at the crack tip accessible to solvent X_{solv} and the length of each crack increment N_L [Dove, 1995]. Hence the creation of new surface area can be viewed as a direct consequence of crack propagation by the bond breaking mechanism [Dunning et al., 1994].

[32] Much of the stress corrosion theory and the experiments in the literature reviewed in the introduction are concerned with the propagation of a single crack in a double torsion type loading apparatus. In our triaxial tests, however, deformation proceeds by the propagation and coalescence of several axial microcracks [Gueguen and Palciauskas, 1994]. Microcrack damage and silica signal are observed to increase in an exponential fashion (15) thus implying accelerating fracture and Si dissolution rates. Such an increase in reaction rates during dilatancy is predicted by both reaction rate theories of active crack growth [Charles and Hillig, 1962; Wiederhorn and Boltz, 1970; Freiman, 1984; Atkinson and Meredith, 1987a; Lawn, 1993] and due to the passive presence of dissolved constituents (Table 2). Increased Si dissolution rates caused by the presence of alkali cations have been observed in numerous studies [Dove and Crerar, 1994; Bennett, 1991; Berger et al., 1994]. Similarly, reaction rate theories predict an exponential increase in reaction rate with applied mean stress as observed here. In contrast, there are various other factors influencing dissolution and fracture rates, whose relative contributions cannot be separated by analyzing experimental data [Dove, 1994; 1995]. For instance, the changes in

X_{solv}, the standard activation entropy ΔS, and the activity coefficients γ_i of H_2O and the reactive intermediates cannot be measured using present techniques. However, it is probable that the surface created by fracturing will lead to an increased number of reactive surface sites X_{solv}, hence increasing the amount of dissolved Si in the pore water.

[33] Our observation of increasing Si concentration during dilatancy show significant differences with the experimental results of Ngwenya et al. [2000]. They observed no strong increase in the amount of dissolved silica during the tertiary creep of Locharbriggs sandstone. In our dynamic loading tests dilatancy was consistently associated with an increased amount of dissolved silica. This discrepancy may have been caused by the differences in the loading configuration or sampling times for the exit pore fluid. It has been suggested that crack growth is inherently faster under constant strain rate tests than creep loading [Kranz, 1979; Rao and Kusunose, 1995], which may lead to the systematic differences in the geochemical signal we observe.

6. Conclusion

[34] The results of our dynamic loading tests demonstrate that the strength of Locharbriggs sandstone depends systematically on the test environment and applied loading rate. We can attribute this observation uniquely to time-dependent fracturing by stress corrosion mechanism. This view is supported by the concomitant exponential increase in silica concentrations indicating chemical corrosion and cumulative AE event rate indicating crack growth and coalescence during strain hardening deformation. In addition, the loading rates used are in the region at which stress corrosion is considered to operate. The observed exponential increase in silica concentrations and AE event rate during strain hardening phase implies that the velocity of crack propagation is directly proportional to the crack length c or the strain energy release rate G under constant loading rate conditions. The microcrack damage inferred from the AE event data is directly correlated to the measured geochemical signal by a power law formulation, with a power law exponent that implies that the reactivity is not proportional to the crack surface area. The low value of the exponent indicates that reaction rates are not uniform for cracks of different ages.

References

Anderson, O. L., and P. C. Grew, Stress corrosion theory of crack propagation with applications to geophysics, *Rev. Geophys.*, 15, 77–104, 1977.

Atkinson, B. K., Subcritical crack propagation in rocks: Theory, experimental results and applications, *J. Struct. Geol.*, 4, 41–56, 1982.

Atkinson, B. K., Subcritical crack growth in geological materials, *J. Geophys. Res.*, 89, 4077–4114, 1984.

Atkinson, B. K., and P. G. Meredith, The theory of subcritical crack growth with applications to minerals and rocks, in *Fracture mechanics of rock*, edited by B. K. Atkinson, pp. 111–166, Academic, San Diego, Calif., 1987a.

Atkinson, B. K., and P. G. Meredith, Experimental fracture mechanics data for rocks and minerals, in *Fracture Mechanics of Rock*, edited by B. K. Atkinson, pp. 477–525, Academic, San Diego, Calif., 1987b.

Barnett, R. L., and R. Kerrich, Stress corrosion cracking in biotite and feldspar, *Nature*, 283, 185–187, 1980.

Bennett, P. C., Quartz dissolution in organic-rich aqueous systems, *Geochim. Cosmochim. Acta*, 55, 1781–1798, 1991.

Berger, G., E. Cadore, J. Schott, and P. M. Dove, Dissolution rate of quartz in lead and sodium electrolyte solutions between 25 and 300°C: Effect of the nature of surface complexes and reaction affinity, *Geochim. Cosmochim. Acta*, 58, 541–551, 1994.

Brady, P. V., and J. V. Walther, Kinetics of quartz dissolution at low temperatures, *Chem. Geol.*, 82, 253–264, 1990.

Bruner, W. M., Comment on "Seismic velocities in dry and saturated cracked solids" by J. O'Connell and Bernard Budiansky, *J. Geophys. Res.*, 81, 2573–2578, 1976.

Charles, R. J., Static fatigue of glass, *J. Appl. Phys.*, 29, 1549–1560, 1958.

Charles, R. J., and W. B. Hillig, Kinetics of glass failure of stress corrosion, in *Symposium sur la Resistance du Verre et les Moyens de l'Ameliorer*, pp. 511–527, Union Sci. Continentale du Verre, Charleroi, Belgium, 1962.

Cox, S. J., and P. G. Meredith, Microcrack formation and material softening in rock measured by monitoring acoustic emissions, *Int. J. Rock Mech. Min. Sci. Geomech Abstr.*, 30, 11–24, 1993.

Crampin, S., E. M. Chesnokov, and R. G. Hipkin, Seismic anisotropy—The state of the art, *Geophys. J. R. Astron. Soc.*, 76, 1–16, 1984.

Darot, M., and Y. Gueguen, Slow crack growth in minerals and rocks: Theory and experiments, *Pure Appl. Geophys.*, 124, 677–692, 1986.

Das, S., and C. H. Scholz, Theory of time-dependent rupture in the earth, *J. Geophys. Res.*, 86, 6039–6051, 1981.

Dove, P. M., Dissolution kinetics of quartz in sodium chloride solutions at 25 to 300°C, *Am. J. Sci.*, 294, 665–712, 1994.

Dove, P. M., Geochemical controls on the kinetics of quartz fracture at subcritical tensile stresses, *J. Geophys. Res.*, 100, 22,349–22,359, 1995.

Dove, P. M., and D. A. Crerar, Kinetics of quartz dissolution in electrolyte solutions using a hydrothermal mixed flow reactor, *Geochim. Cosmochim. Acta*, 54, 955–969, 1990.

Dove, P. M., and J. D. Rimstidt, Silica-water interactions, in *Silica—Physical Behaviour, Geochemistry and Materials Applications*, edited by P. J. Heaney, C. T. Prewitt, and C. V. Gibbs, pp. 259–308, Mineral. Soc. of Am., Washington, D. C., 1994.

Dullien, F. A. L., *Porous Media*, Academic, San Diego, Calif., 1979.

Dunning, J., B. Douglas, M. Miller, and S. McDonald, The role of the chemical environment in frictional deformation: Stress corrosion cracking and comminution, *Pure Appl. Geophys.*, 143, 151–178, 1994.

Dunning, J. D., W. L. Lewis, and D. E. Dunn, Geomechanical weakening in the presence of surfactants, *J. Geophys. Res.*, 85, 5344–5354, 1980.

Dunning, J. D., D. Petrovski, J. Schuyler, and A. Owens, The effects of aqueous chemical environments on crack propagation in quartz, *J. Geophys. Res.*, 89, 4115–4123, 1984.

Franklin, S. P., T. A. Dewers, and T. T. Tieh, The role of carboxylic acids in albite and quartz dissolution: An experimental study under diagenetic conditions, *Geochim. Cosmochim. Acta*, 58, 4259–4279, 1994.

Freiman, S. W., Effects of chemical environments on slow crack growth in glasses and ceramics, *J. Geophys. Res.*, 89, 4072–4076, 1984.

Gueguen, Y., and V. Palciauskas, *Introduction to the Physics of Rocks*, Princeton Univ. Press, Princeton, N. J., 1994.

Holdren, G. R., Jr., and P. M. Speyer, Reaction rate-surface area relationships during the early stages of weathering II. Data on eight additional feldspars, *Geochim. Cosmochim. Acta*, 51, 2311–2318, 1987.

John, M., The influence of loading rate on mechanical properties and fracture processes of rock, *CSIR Rep. ME 1115*, Counc. for Sci. and Ind. Res., Pretoria, South Africa, 1972.

Kanamori, H., and D. L. Anderson, Theoretical basis of some empirical relations in seismology, *Bull. Seismol. Soc. Am.*, 65, 1073–1095, 1975.

Kieffer, B., C. F. Jove, E. H. Oelkers, and J. Schott, An experimental study of the reactive surface area of the Fontainebleau sandstone as a function of porosity, permeability and fluid flow rate, *Geochim. Cosmochim. Acta*, 63, 3525–3534, 1999.

Kirby, S. H., Introduction and digest to the special issue on chemical effect of water on the deformation and strengths of rocks, *J. Geophys. Res.*, 89, 3991–3995, 1984.

Kranz, R. L., Crack growth and development during creep of Barre granite, *Int. J. Rock Mech. Min. Sci. Geomech. Abstr.*, 16, 23–35, 1979.

Krausz, A. S., The deformation and fracture kinetics of stress corrosion cracking, *Int. J. Fract.*, 14, 5–15, 1978.

Krausz, A. S., and H. Eyring, *Deformation Kinetics*, Wiley-Interscience, New York, 1975.

Lankford, J., The role of tensile microfracture on the strain rate dependence of compressive strength of fine-grained limestone—Analogy with strong ceramics, *Int. J. Rock Mech. Min. Sci. Geomech Abstr.*, 18, 173–175, 1981.

Lawn, B., *Fracture of brittle solids*, 2nd ed., Cambridge Univ. Press, New York, 1993.

Lei, X., K. Kusunose, M. V. M. S. Rao, O. Nishizawa, and T. Satoh, Quasi-static fault growth and cracking in homogeneous brittle rock under triaxial compression using acoustic emission monitoring, *J. Geophys. Res.*, 105, 6127–6139, 2000.

Lockner, D. A., The role of acoustic emission in the study of rock fracture, *Int. J. Rock Mech. Min. Sci. Geomech. Abstr.*, 30, 883–899, 1993a.

Lockner, D. A., Room temperature creep in saturated granite, *J. Geophys. Res.*, 98, 475–487, 1993b.

Lockner, D. A., A generalised law for brittle deformation of Westerley granite, *J. Geophys. Res.*, 103, 5107–5123, 1998.

Main, I. G., A modified Griffith criterion for the evolution of damage with a fractal distribution of crack lengths: Application to seismic event rates and b-values, *Geophys. J. Int.*, 107, 353–362, 1991.

Main, I. G., Applicability of time-to-failure analysis to accelerated strain before earthquakes and volcanic eruptions, *Geophys. J. Int.*, 139, F1–F6, 1999.

Main, I. G., A damage mechanics model for power-law creep and earthquake aftershock and foreshock sequences, *Geophys. J. Int.*, 142, 151–161, 2000.

Main, I. G., and P. G. Meredith, Stress corrosion constitutive laws as a possible mechanism for intermediate-term and short-term seismic quiescence, *Geophys. J. Int.*, 107, 363–372, 1991.

Mair, K., I. Main, and S. Elphick, Sequential growth of deformation bands in the laboratory, *J. Struct. Geol.*, 22, 25–42, 2000.

Martin, R. J., III, Time-dependent crack growth in quartz and its application to the creep of rocks, *J. Geophys. Res.*, 77, 1406–1419, 1972.

Masuda, K., Effects of water on rock strength in a brittle regime, *J. Struct. Geol.*, 23, 1653–1657, 2001.

Meredith, P. G., and B. K. Atkinson, Stress corrosion and acoustic emission during tensile crack propagation in Whin Sill dolerite and other basic rocks, *Geophys. J. R. Astron. Soc.*, 75, 1–21, 1983.

Meredith, P. G., I. G. Main, and C. Jones, Temporal variations in seismicity during quasi-static and dynamic rock failure, *Tectonophysics*, 175, 249–268, 1990.

Mogi, K., Study of elastic shocks caused by the fracture of heterogeneous materials and its relation to earthquake phenomena, *Bull. Earthquake Res. Inst. Univ. Tokyo*, 40, 125–173, 1962.

Ngwenya, B. T., S. C. Elphick, I. G. Main, and G. B. Shimmield, Experimental constraints on the diagenetic self-sealing capacity of faults in high porosity rocks, *Earth Planet. Sci. Lett.*, 183, 187–199, 2000.

Obert, L., and W. Duvall, Use of subaudible noises for the prediction of rock bursts, part II, *U.S. Bur. Mines Rep. 3654*, 1942.

Parks, G. A., Surface and interfacial free energies of quartz, *J. Geophys. Res.*, 89, 3997–4008, 1984.

Paterson, M. S., The thermodynamics of water in quartz, *Phys. Chem. Miner.*, 13, 245–255, 1986.

Rao, M. V. M. S., and K. Kusunose, Failure zone development in andesite as observed from acoustic emission locations and velocity changes, *Phys. Earth Planet. Inter.*, 88, 131–143, 1995.

Renshaw, C. E., and D. D. Pollard, Numerical simulation of fracture set formation: A fracture mechanics model consistent with experimental observations, *J. Geophys. Res.*, 99, 9359–9372, 1994.

Reuschle, T., M. Darot, and Y. Gueguen, Mechanical and transport properties of crustal rocks: From single cracks to crack statistics, *Phys. Earth Planet. Inter.*, 55, 353–360, 1989.

Rice, J. R., Thermodynamics of the quasi-static growth of Griffith cracks, *J. Mech. Phys. Solids*, 26, 61–78, 1978.

Rimstidt, J. D., and H. L. Barnes, The kinetics of silica-water interactions, *Geochim. Cosmochim. Acta*, 44, 1683–1699, 1980.

Sangha, C. M., and R. K. Dhir, Influence of time to the strength, deformation and fracture properties of a lower devonian sandstone, *Int. J. Rock Mech. Min. Sci.*, 9, 343–354, 1972.

Sano, O., I. Ito, and M. Terada, Influence of strain rate on dilatancy and strength of Oshima granite under uniaxial compression, *J. Geophys. Res.*, 86, 9299–9311, 1981.

Scholz, C. H., Microfracturing and the inelastic deformation of rock in compression, *J. Geophys. Res.*, 73, 1417–1432, 1968.

Scholz, C. H., Static fatigue of quartz, *J. Geophys. Res.*, 77, 2104–2114, 1972.

Schultz, R. A., Growth of geologic fractures into large-strain populations: Review of nomenclature, subcritical crack growth and some implications for rock engineering, *Int. J. Rock Mech. Min. Sci.*, 37, 403–411, 2000.

Segall, P., Rate-dependent extensional deformation resulting from crack growth in rock, *J. Geophys. Res.*, 89, 4185–4195, 1984.

Serdengecti, S., and G. D. Boozer, The effects of strain rate and temperature on the behavior of rocks subjected to triaxial compression, in *Proceedings of the Fourth Symposium on Rock Mechanics*, pp. 83–97, Pa. State Univ., University Park, 1961.

Swanson, P. L., Subcritical crack growth and other time and environment-dependent behavior in crustal rocks, *J. Geophys. Res.*, *89*, 4137–4152, 1984.

Walsh, J. B., The effect of cracks on the compressibility of rock, *J. Geophys. Res.*, *70*, 381–389, 1965.

Wiederhorn, S. M., and L. H. Boltz, Stress corrosion and static fatigue of glass, *J. Am. Ceram. Soc.*, *53*, 543–548, 1970.

―――――――――――

S. C. Elphick, I. G. Main, B. T. Ngwenya, and I. O. Ojala, School of GeoSciences, University of Edinburgh, Grant Institute, West Mains Road, Edinburgh, EH9 3JW, UK. (stephen.elphick@glg.ed.ac.uk; ian.main@glg.ed.ac.uk; bryne.ngwenya@glg.ed.ac.uk; ira.ojala@glg.ed.ac.uk)